ELSEVIER

Physics of the Earth and Planetary Interiors 119 (2000) 185–208

PHYSICS OF THE EARTH AND PLANETARY INTERIORS

www.elsevier.com/locate/pepi

Seismic properties of the Eltanin Transform System, South Pacific

Emile A. Okal *, Amy R. Langenhorst [1]

Department of Geological Sciences, Northwestern University, Evanston, IL 60208, USA

Received 13 May 1999; accepted 10 November 1999

Abstract

We present a compilation of the seismic properties of the Eltanin Transform Fault (TF) system, compelled by the recent discovery of the Hollister Ridge and the possibility of a change of plate kinematics pattern in the region. The Hollister Ridge is a major volcanic system located on the Western flank of the Pacific–Antarctic Ridge (PAR), immediately south of the Eltanin Fracture Zones (FZs). We find or confirm two anomalous characteristics: the occurrence of seven normal faulting events on the transform segments, expressing extension across the plate boundary in the azimuth N26°W, and more than 90% deficiency in the seismic moment released during strike–slip events on the transforms, as compared to the rate expected from kinematic models. Other seismic properties are typical of the seismicity of a fast-spreading mid-ocean ridge (MOR) system. In particular, we could not document a single teleseismically recorded event on the Hollister Ridge; earthquakes are confined to narrow TFs with no activity present on the ridge segments. The transform events have regular frequency–moment statistics, and we could not document any significantly slow sources. These seismic properties generally support conventional plate tectonics models such as NUVEL-1, and cannot be reconciled with a proposed reorientation of the Pacific plate 4 Ma ago.

Keywords: Seismic properties; Eltanin Transform System; South Pacific

1. Introduction and background

The purpose of this paper is to review a number of seismic properties of the Eltanin Transform Fault (TF) and adjoining areas (Fig. 1), in the wake of the 1996 discovery of the Hollister Ridge, and of the ensuing debate about its possible relationship to the Louisville hotspot (Wessel and Kroenke, 1997; Vlastelic et al., 1998).

The Hollister Ridge is a large volcanic feature extending on the western flank of the Pacific–Antarctic Ridge (PAR). Anomalous bathymetry was first detected in the area during the 1965 cruise of *R/V Eltanin*, which identified a sounding of only 260 m bsl at 53.9°S, 140.3°W. Later exploration by Natland et al. (1995) revealed additional shallow soundings, which, these authors suggested, made up a chain of seamounts that they named the Hollister Ridge. The ridge also has a definite signature in the geoid, described in detail by Small (1995). In the meantime, intense volcanoseismic activity was identified during 1991–1993 in the form of *T* phases

* Corresponding author.

[1] Now at: Institut für Geowissenschaften, Universität Potsdam Karl-Liebknecht Str. 24, Golm D-14467, Germany.

0031-9201/00/$ - see front matter
PII: S0031-9201(99)00169-7

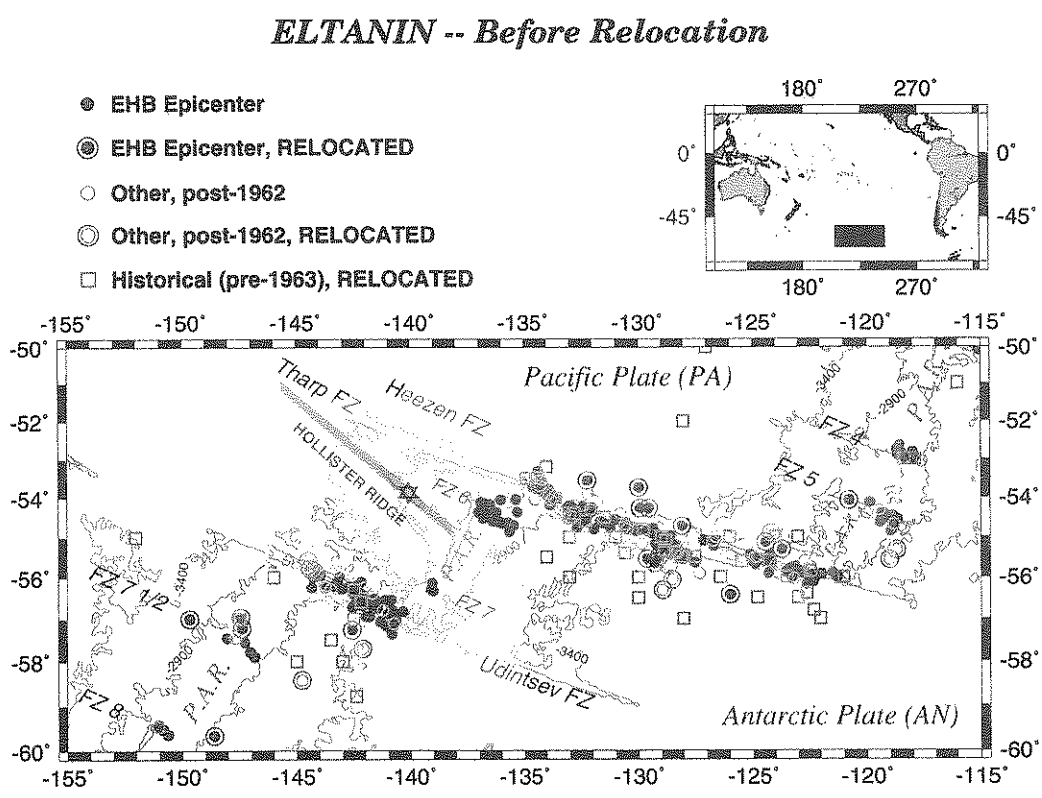

Fig. 1. Location map of the study area, with published seismicity (before relocation). The principal fracture zones are identified, as are segments of the PAR. The isobaths are drawn at 500 m intervals between 1900 and 3400 m, from the dataset of Smith and Sandwell (1995). The shaded area is the "Hollister region" whose seismicity is detailed in Fig. 3 and studied separately. The Hollister Ridge is showed symbolically as the darker trace joining the Tharp FZ and the PAR. Bulletin epicenters shown with various symbols (see text for details). In addition, the Star of David shows the location of the 1991–1992 acoustic swarm studied by Talandier and Okal (1996). The small map at upper right replaces the main map (solid rectangle) in the Pacific Basin at large.

recorded at Polynesian seismic stations (Talandier and Okal, 1996), which led to a comprehensive shipboard exploration of the region by *N/O l'Atalante* in February 1996. As a result, the Hollister Ridge was mapped as a massive feature extending 440 km in a N48°W direction from the PAR at 55°S, 138°W to its termination near the Eltanin Fracture Zone (FZ) system, at 52.3°S, 143.5°W. A structurally continuous central segment was identified with a length of 200 km, a base width of 23 km, and a shallowest sounding at 100 m bsl (Vlastelic et al., 1998); the scale and height of the structure make it unique among the basaltic edifices on the floor of the world's oceans.

The exact origin of the Hollister Ridge is, at present, unknown. Wessel and Kroenke (1997) have speculated that a change in motion of the Pacific plate over the mantle took place ~4 Ma ago, and thus proposed that the Hollister Ridge constitutes the most recent track of the Louisville hotspot over the Pacific plate. However, Vlastelic et al. (1998) have argued that the isotopic signature of basalts dredged on the Hollister Ridge can be explained neither by direct tapping of the Louisville reservoir (as defined from older seamounts in the chain), nor by a simple mixing of Louisville hotspot and Pacific–Antarctic MORB materials. Thus, the tectonic regime responsible for the development and growth of the Hollister Ridge is unclear.

In addition to the suggestion of Wessel and Kroenke (1997) of a change of absolute motion of the Pacific plate, the evolution of spreading along the

PAR has been the subject of several studies, notably by Stock and Molnar (1982). More recently, Cande et al. (1995) gave evidence for a gradual evolution of the Pacific–Antarctic rotation vector culminating in an abrupt 8° clockwise change 5.9 Ma ago. In this general framework, we note that the Eltanin FZ system constitutes, by far, the largest geographical offset in the Southern boundary of the Pacific plate, with the portion of the Pacific plate south of the Louisville Ridge being peninsular in shape. A legitimate question then arises as to whether that Southern section remained rigidly attached to the main part of the plate during the reorientations, or whether some form of relative motion developed at that time across a boundary grossly located at the non-TF part of the Eltanin FZ; this could have led to a pinching of the lithosphere possibly related to the generation of the Hollister Ridge. Similarly, in such circumstances, the Eltanin TF system may have developed into a diffuse or ''leaky'' boundary, a configuration which, if still ongoing, may explain its notorious deficiency in seismic activity, as identified by Stewart and Okal (1983).

In the general context of any future model for the origin of the Hollister Ridge, it is important to re-examine the various aspects of the seismicity of the entire Hollister–Eltanin region, since one would generally expect processes, such as the building of a massive volcanic structure, or the tearing off of a large portion of the Pacific plate, to translate into detectable seismological properties, affecting both the location and the mechanism of local earthquakes. In the present paper, we review the location of the earthquakes, their frequency size characteristics, their focal mechanisms along the TF segments, their source slowness, and the relation of the total seismic moment release to that expected from plate kinematic models. We conclude that the only anomalous characteristics of the region's seismicity are the deficiency in moment release along the local TFs and the presence of a few normal faulting earthquakes; however, the latter cannot be taken as proof of an irregular regime of plate kinematics, given the low level of moment release involved.

1.1. Previous studies

The seismicity of the Eltanin system was analyzed by Stewart and Okal (1983), with the goal of quantifying the deficiency in seismic moment release with respect to the motion expected from plate kinematic models; these authors did not attempt any systematic relocation of the events. Okal (1984) and later Wysession et al. (1991) relocated the intraplate seismicity of the Pacific Basin; since they focused on intraplate events, they did not relocate earthquakes whose bulletin epicenter was less than 2° from a plate boundary. Finally, as part of their study of the volcanic swarm at the Hollister site, Talandier and Okal (1996) compiled the seismicity of a small region surrounding the Hollister Ridge.

In parallel, Wolfe et al. (1993) studied the occurrence of earthquakes with anomalous focal mechanisms worldwide along the Mid-Oceanic Ridge (MOR) system, and documented five such events in the Eltanin region. Later, and following detailed shipboard geophysical surveying of the Eltanin system, Lonsdale (1994) interpreted small-scale features of the region's morphology in the context of the Pliocene reorientation of Pacific–Antarctic spreading.

2. Seismicity and relocation

The purpose of this section is twofold: First, we study the seismicity of the Eltanin and Udintsev transform systems, looking for any evidence suggestive of a diffuse, ''leaky'' boundary; such a pattern could, if present, be indicative of a lack of rigidity in the plates bordering the transforms. In addition, we investigate any possible teleseismic activity in the immediate vicinity of the Hollister Ridge, both on the Pacific–Antarctic plate boundary, and along the Hollister structure itself. Ridge segments along the entire Pacific–Antarctic system, north of 63°S, are opening at a full rate of 6–10 cm/year, and as such feature the lack of teleseismic events characteristic of fast-spreading ridges (Stein and Woods, 1989). Any earthquake locating on the ridge segment between the Udintsev and Eltanin transform systems would violate this pattern, and thus indicate an anomalous tectonic regime. Similarly, it is important to document whether any seismicity can be associated with the intraplate segment of the Hollister Ridge. The ''Hollister region'' will be defined as the shaded area on Fig. 1.

For practical purposes, we delineate a study area bounded by latitudes 60°S and 50°S, and longitudes 155°W and 115°W. We refer to Molnar et al. (1975) and adopt their nomenclature of FZs along the East Pacific Rise. As shown on Fig. 1, the principal FZs are, from the north: the Menard FZ (cutting through the corner of the map at 50°S, 115°W); FZs 4 and 5 (the former the single left-lateral offset); the Eltanin system, composed of two main FZs, the Heezen and Tharp FZs, separated at 127°W; FZs 6 and 7, the former only 70 km Southwest of the Tharp (the latter defined by a cluster of seismicity at 56°S, 139°W); the Udintsev FZ, centered at 57°S, 142°W; and FZ 8, centered at 60°S, 150°W. Between the Udintsev and FZ 8 systems, seismicity, and to a lesser extent the sparse available bathymetry, define an additional FZ, centered at 58°S, 147°W, and not part of the nomenclature of Molnar et al. (1975). Following common usage in marine geophysics (e.g., Cande et al., 1995), we interpolate the nomenclature, and refer to this feature as ''FZ 7 1/2''. Note finally that Lonsdale (1994) names TFs 5 and 6 as the ''Raitt'' and ''Hollister'' TFs, respectively.

2.1. Methodology

Our relocations are based on arrival times listed in the *International Seismological Summary* (ISS) for 1920–1956, its successor, the *Bulletin of the International Seismological Center* (ISC) since 1964, and the *Bulletin du Centre International de Séismologie* (BCIS) during the lean years of the ISS (1957–1963). They use the iterative interactive algorithm described in detail by Wysession et al. (1991), including its estimation of uncertainties using a Monte Carlo method consisting of injecting Gaussian noise into the dataset, the standard deviation of the noise, σ_G, varying from 1 s for modern earthquakes to 10 s in the 1920s. For events in 1995 for which ISC data are not yet available, we retrieved phase data from the National Earthquake Information Center (NEIC) web site. We note, however, that such datasets are generally smaller than their ISC counterparts, and that the resulting relocations may be less precise. For this reason, we do not relocate small events occurring in 1996 or later. Finally, it should be borne in mind that all earthquakes in the study area lack nearby stations, resulting in large error bars and generally unresolvable source depths. Consequently, we constrained all relocations to a depth of 10 km.

In their previous study, Talandier and Okal (1996) examined 38 earthquakes (spanning the years 1930–1993) initially located between 135°W and 140.5°W, and concluded that no events detected teleseismically were known, either on the Hollister Ridge itself, or on the spreading segment between transforms 6 and 7.

Since that study was published, Engdahl et al. (1998) released their new worldwide catalogue of relocated hypocenters (hereafter, EHB). Because it is based on the refined IASPEI-91 travel times (Kennett and Engdahl, 1991) and makes use of all available seismic arrivals without identifying phases a priori, this dataset is of superior quality, and should, in principle, obviate the need for reassessment of seismicity for the years covered (1964–1995). However, it suffers from a relatively high magnitude threshold for completeness (as high as $m_b \geq 5.4$ in the region under study). We therefore proceeded to compare the epicenters obtained by Talandier and Okal (1996) with the EHB relocations: for a dataset of 14 common events, we find an average distance between epicenters of only 14 km, and a maximum one of 35 km. This independent check justifies the use of the relocation procedure, as described by Wysession et al. (1991), to complement the EHB catalogue for historical events and for smaller earthquakes falling below their threshold of study.

2.1.1. The seismicity of the Eltanin and Udintsev Systems

The seismicity of the Eltanin, Udintsev and adjoining TF systems, as obtained from catalogue sources, and before relocation, is shown on Fig. 1. Except for the EHB epicenters, this figure does not include events in the shaded Hollister region, which is studied separately in Section 2.1.2. A description of the 82 events chosen for relocation is given in Appendix A. Relocation results are shown on Fig. 2 and listed in Table 1, with details available in Appendix A. It is clear from a comparison of the two figures that the transverse extent of the seismicity along the transform segments is considerably less

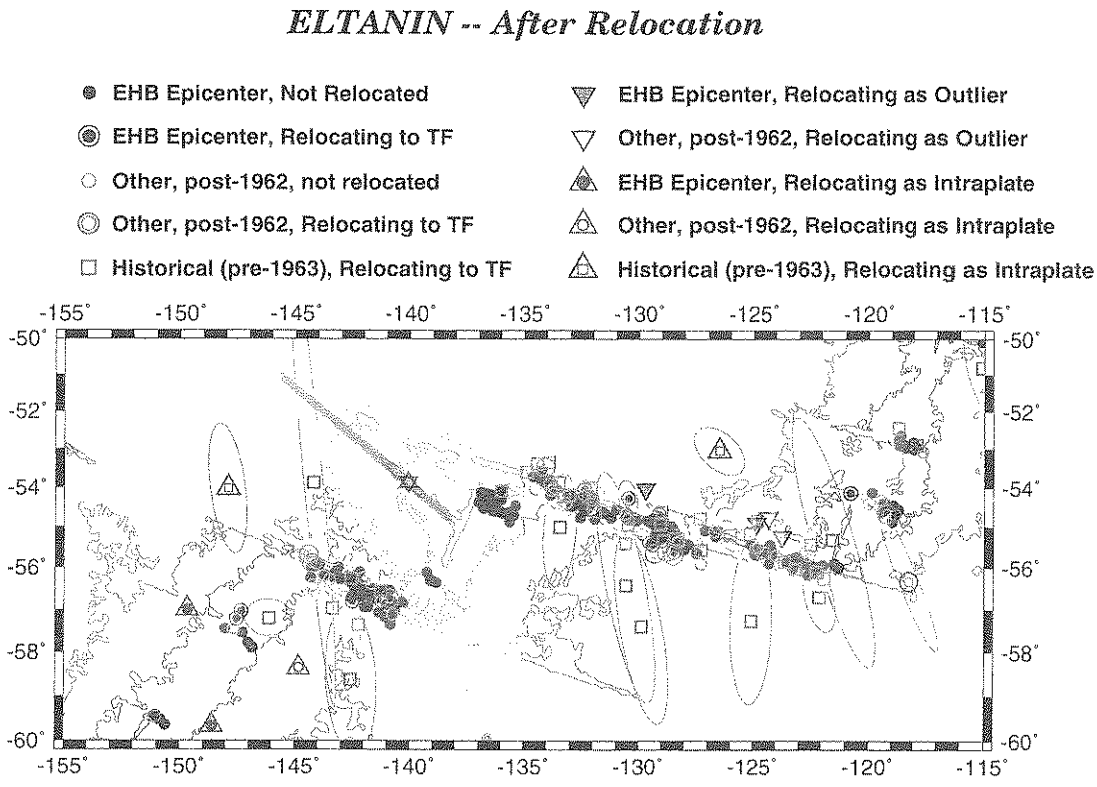

Fig. 2. Seismicity of the Eltanin area after relocation. See Fig. 1 and text for details.

than the 200 km suggested by Fig. 1. The picture emerging from the relocation of Eltanin seismicity is that of narrow lines of activity along well-defined TF segments; no zone of diffuse seismicity is identified. The only exception to this pattern is the presence of five "outlier" earthquakes on supposedly inactive segments of the Heezen FZ, which will be further discussed below.

2.1.2. Seismicity of the Hollister region

Fig. 3 similarly presents the seismicity of the Hollister region, defined as all events with original bulletin locations between 135°W and 140.5°W. Details of the 28 events targeted for relocation are given in Appendix A, with Fig. 4 and Table 2 providing the final epicentral data.

The result of this effort is that we fail to document any activity detectable from conventional seismic waves (as opposed to the acoustic waves reported by Talandier and Okal, 1996), along either the Hollister Ridge or the nearby segment of PAR. We must conclude that whatever tectonic processes may remain involved in the growth of the Hollister Ridge take place in a seismically quiet fashion, at least above the threshold of completeness for teleseismic detection in this province. The latter is estimated at no better than $m_b \geq 4.7$, based on frequency–magnitude relations. When considering the Udintsev and Eltanin systems on a larger scale, their seismicity is arranged along clearly defined transform segments; no earthquakes could be found on the presumed ridge segments located between the Udintsev and Tharp transforms at 135°W, and between the Tharp and Heezen transforms at 127°W.

2.2. Discussion

In Fig. 5, we show a close-up of the central section of our study area. This figure clearly docu-

Table 1
Relocation of Eltanin dataset
Note that all relocations were carried out at a constrained depth of 10 km; NS is the number of stations used in the relocation, σ the resulting root-mean-squared residual. An event is listed as "relocating to the TF system" if its Monte Carlo ellipse intersects at least one TF segment. M_{PAS}: "Pasadena" magnitude assigned by Gutenberg and Richter (1954) or, subsequently, by the Pasadena Seismological Observatory; M_{MAT}: magnitude assigned by Matsushiro Observatory.

Date	Original (bulletin) location					Result of relocation				
Day Month (J) Year	Time (GMT)	Epicenter (°N)	(°E)	Depth (km)	Magnitude	Epicenter (°N)	(°E)	Time (GMT)	NS	σ (s)
Targeted EHB events relocating to TF systems										
19 April (110) 1964	3:44:57.1	−53.74	−129.98	10	4.8 m_b	−54.69	−129.10	3:44:51.7	12	2.14
27 December (361) 1967	0:27:27.4	−53.56	−132.22	2	4.9 m_b	−54.04	−132.38	0:27:26.2	14	1.10
30 December (365) 1968	9:12:13.1	−55.50	−129.10	12	4.8 m_b	−55.62	−128.47	9:12:13.0	19	3.19
29 January (029) 1972	6:16:59.8	−55.65	−129.28	10		−55.43	−129.39	6:16:57.9	18	2.07
14 July (196) 1980	21:24:10.9	−57.26	−142.59	1	4.8 m_b	−56.80	−142.51	21:24:11.2	32	2.79
28 February (059) 1985	0:15:35.5	−55.55	−129.62	5	4.7 m_b	−55.38	−129.52	0:15:35.1	16	2.54
29 July (211) 1992	1:54:57.2	−56.42	−125.99	10	5.3 m_b	−54.84	−129.01	1:54:46.4	19	1.80
22 October (295) 1993	18:26:12.5	−54.08	−120.77	10	4.5 m_b	−54.14	−120.78	18:26:11.6	10	0.83
1 November (305) 1993	3:19:58.2	−56.96	−147.45	6	4.4 m_b	−57.04	−147.34	3:19:58.3	20	2.18
5 August (217) 1994	19:41:58.7	−54.72	−128.06	1	5.0 m_b	−55.11	−128.55	19:41:56.9	34	2.66
25 March (084) 1995	17:21:50.9	−57.23	−147.41	15	4.2 m_b	−57.22	−147.53	17:21:49.1	8	1.50
12 December (346) 1995	22:39:26.3	−54.27	−129.92	9	4.6 m_b	−54.27	−130.47	22:39:26.8	10	2.17
Targeted EHB events relocating intraplate										
23 November (327) 1985	12:45: 7.4	−59.67	−148.61	7	5.4 m_b	−59.55	−148.68	12:45: 6.4	28	1.10
21 December (355) 1987	19:46:26.8	−57.00	−149.67	10	5.1 m_b	−56.83	−149.85	19:46:25.8	13	1.30
Targeted EHB events relocating as outliers										
16 August (229) 1984	15:31: 0.8	−55.31	−123.71	10	5.3 m_b	−55.24	−123.74	15:31: 0.1	30	0.85
26 July (207) 1987	23:17:47.4	−55.14	−124.44	26	4.7 m_b	−54.91	−124.87	23:17:43.9	12	2.27
10 April (100) 1993	13:31: 2.5	−54.27	−129.54	3	4.7 m_b	−54.04	−129.70	13:31: 1.6	11	0.96
Modern, non-EHB, events relocating on TF systems										
10 January (010) 1968	13:42: 6.2	−53.70	−134.30	33	4.8 m_b	−53.47	−134.07	13:42: 4.2	12	1.94
24 November (328) 1970	12:22:16.3	−55.58	−144.49	33	5.4 m_b	−55.89	−144.28	12:22:16.3	12	2.19
10 June (161) 1973	7:16:19.5	−57.70	−142.12	33	5.2 m_b	−56.75	−140.88	7:16:15.0	12	3.54
5 February (036) 1975	2:34:53.0	−55.57	−119.01	33	4.8 m_b	−54.67	−119.22	2:34:52.5	9	1.65
27 November (331) 1982	2:50:46.1	−55.84	−144.23	10	5.4 m_b	−55.69	−144.40	2:50:46.1	13	1.23
27 November (331) 1982	3:30:42.3	−55.79	−144.40	10	5.1 m_b	−55.68	−144.43	3:30:42.9	9	1.15
9 January (009) 1986	15:49:37.6	−55.71	−128.67	10	5.2 M_s	−55.60	−128.79	15:49:38.5	10	2.85
21 June (172) 1990	10:21:35.0	−56.07	−128.49	10	5.0 m_b	−55.70	−128.49	10:21:36.2	9	0.87
30 January (030) 1993	11:5:29.2	−55.34	−118.71	10	5.3 M_s	−56.33	−118.22	11: 5:30.2	5	0.86
6 August (218) 1994	3:27:15.5	−56.31	−128.94	10	5.3 M_s	−55.65	−129.31	3:27:16.5	13	1.30
Modern, non-EHB, event relocating intraplate										
9 December (343) 1990	11: 8:58.9	−58.43	−144.77	10	4.9 m_b	−58.36	−144.84	11: 8:59.6	6	0.86
Modern, non-EHB, event relocating as outlier										
9 October (282) 1966	12: 6:42.6	−54.90	−124.20	33	4.7 m_b	−54.77	−124.33	12:6:39.2	9	0.57
Five specially targeted events defining TF 5 1 / 2										
12 November (316) 1965	2:4:18.1	−55.99	−121.29	13	4.5 m_b	−55.89	−121.19	2:4:16.7	23	2.27
14 August (227) 1980	5:5:55.4	−55.91	−121.46	8	5.0 m_b	−55.86	−121.61	5:5:53.7	31	1.08
09 April (099) 1995	0:52:15.8	−55.93	−121.97	19	4.1 m_b	−55.83	−122.04	0:52:13.0	11	1.14
08 May (128) 1965	3:53:59.1	−55.60	−122.70	33	4.3 m_b	−55.46	−123.78	3:53:55.2	8	1.49
08 September (251) 1995	1:0:9.5	−55.88	−122.38	10	4.0 m_b	−55.70	−122.57	1:0:9.7	8	1.20

Table 1 (*continued*)

Date	Original (bulletin) location					Result of relocation				
Day Month (J) Year	Time (GMT)	Epicenter (°N)	Epicenter (°E)	Depth (km)	Magnitude	Epicenter (°N)	Epicenter (°E)	Time (GMT)	NS	σ (s)
Historical events relocating on TF system										
16 February (047) 1929	19:23:16.0	−56.00	−121.00	0	6.25 M_{PAS}	−55.32	−121.55	19:23:19.5	8	3.80
6 January (006) 1930	23:50:0.0	−55.00	−131.00	0	6.00 M_{PAS}	−56.42	−130.56	23:49:59.1	7	6.44
21 July (203) 1932	16:16:3.0	−55.00	−131.00	0		−54.41	−132.04	16:15:55.1	6	2.52
19 April (109) 1933	1:45:47.0	−51.00	−116.00	0	6.00 M_{PAS}	−50.81	−115.09	1:45:55.3	10	3.62
16 May (136) 1935	20:41:30.0	−55.00	−123.00	0	6.25 M_{PAS}	−56.09	−122.27	20:41:32.8	15	3.75
13 August (225) 1937	11:47:38.0	−56.50	−130.00	0	6.00 M_{PAS}	−57.40	−129.86	11:47:38.0	10	1.69
20 January (020) 1940	9:58:0.0	−55.00	−133.00	0	6.75 M_{PAS}	−54.08	−136.01	9:58:10.8	10	2.22
14 February (045) 1941	18:55:3.0	−56.00	−133.00	0	6.50 M_{PAS}	−53.99	−132.10	18:55:14.9	11	4.17
13 November (317) 1943	16:43:28.0	−55.00	−129.00	0	6.50 M_{PAS}	−54.91	−129.03	16:43:34.5	14	3.28
1 April (092) 1944	9:22:8.0	−57.00	−128.00	0	6.00 M_{PAS}	−55.30	−128.46	9:22:12.5	11	3.25
3 September (247) 1944	19:11:29.0	−57.00	−122.00	0	7.00 M_{PAS}	−56.71	−122.12	19:11:29.8	17	2.64
22 July (204) 1952	22:50:17.0	−56.80	−122.30	0		−56.26	−121.92	22:50:20.2	10	4.16
7 May (127) 1953	17:56:36.0	−56.50	−124.80	0		−57.26	−125.10	7:16:29.2	13	1.77
20 May (140) 1953	7:45:24.0	−53.20	−134.00	0	7.25 M_{PAS}	−53.34	−133.92	7:45:25.6	25	2.64
15 February (046) 1954	12:15:36.0	−58.00	−145.00	0		−53.88	−144.21	12:15:38.4	5	3.07
19 February (050) 1954	13:54:29.0	−55.50	−134.00	0		−55.00	−133.43	13:54:28.5	11	1.49
28 June (179) 1954	4:57:50.0	−58.80	−142.40	0		−58.63	−142.59	4:57:52.9	14	2.16
19 October (293) 1956	14:5:34.0	−55.86	−122.46	0	6.50 M_{PAS}	−55.43	−122.48	14:5:38.0	19	2.97
20 April (110) 1957	6:48:4.0	−54.50	−131.50	0		−54.60	−131.95	6:48:10.2	14	2.27
2 May (122) 1957	10:34:14.0	−56.50	−123.00	0		−56.02	−123.15	10:34:20.1	22	2.88
24 June (175) 1957	11:1:50.0	−55.50	−127.50	0		−54.78	−127.35	11:1:49.0	9	2.73
18 August (230) 1957	6:34:16.0	−57.00	−142.50	0		−56.55	−141.27	6:34:11.2	13	2.75
20 August (232) 1957	4:48:6.0	−56.00	−130.00	0		−55.18	−126.04	4:47:59.8	6	2.15
9 October (282) 1957	1:25:35.0	−53.50	−134.50	0		−53.38	−134.44	1:25:37.5	6	1.62
7 November (311) 1957	6:21:56.0	−57.50	−143.50	0		−56.97	−143.40	6:21:58.3	14	3.71
26 January (026) 1958	3:35:17.0	−54.50	−133.00	0		−54.23	−133.26	3:35:20.0	12	1.38
18 June (169) 1959	6:50:44.0	−55.34	−128.86	0		−55.34	−128.91	6:50:46.2	16	2.08
29 November (333) 1959	19:17:40.0	−57.00	−147.50	0		−57.21	−146.11	19:17:38.5	10	2.04
19 October (293) 1960	10:31:52.1	−54.80	−129.80	17		−54.94	−130.48	10:31:53.2	9	3.21
17 November (322) 1960	21:22:45.6	−56.40	−122.60	38		−56.12	−122.22	21:22:43.0	14	2.71
18 June (169) 1961	22:13:25.1	−56.60	−142.20	33	5.63 M_{MAT}	−57.36	−142.25	22:13:29.3	16	4.78
2 August (214) 1961	1:17:8.1	−53.50	−134.90	22		−53.59	−134.89	1:17:9.0	18	1.94
17 August (229) 1961	5:6:2.7	−55.60	−125.50	33	5.20 M_{MAT}	−55.16	−125.16	5:5:59.9	9	1.40
17 May (137) 1962	4:8:18.0	−55.10	−128.80	25		−54.94	−129.05	4:8:16.0	9	1.31
3 July (184) 1962	18:13:35.6	−56.30	−142.50	25		−56.27	−142.59	18:13:34.8	22	3.04
3 July (184) 1962	18:22:6.3	−54.60	−132.30	25		−54.22	−132.23	18:22:4.3	17	1.81
25 September (268) 1962	0:21:14.6	−55.60	−124.30	67		−55.63	−124.58	0:21:8.5	29	2.14
2 January (002) 1963	15:55:47.8	−53.00	−117.90	33		−52.90	−117.87	15:55:45.3	25	2.18
16 January (016) 1963	3:14:6.2	−54.00	−133.60	33		−53.87	−133.49	3:14:3.3	22	2.29
3 April (093) 1963	14:47:55.6	−55.50	−128.10	33	5.8 m_b	−54.61	−128.98	14:47:52.9	31	3.78
21 May (141) 1963	0:58:7.4	−56.00	−123.50	33	4.4 m_b	−55.86	−123.64	0:58:2.8	14	2.58
10 August (222) 1963	18:7:26.2	−54.40	−132.80	33	4.7 m_b	−54.19	−133.05	18:7:22.8	20	1.69
6 September (249) 1963	11:58:38.9	−55.40	−128.40	33	4.4 m_b	−55.28	−128.47	11:58:35.3	12	1.21
11 November (315) 1963	7:32:43.2	−56.00	−126.40	33	4.6 m_b	−55.56	−127.30	7:32:37.2	5	2.69
28 December (362) 1963	23:55:7.7	−53.00	−118.40	33	5.0 m_b	−52.44	−118.68	23:55:6.0	12	1.21
Historical events relocating as intraplate										
5 September (248) 1938	14:42:26.0	−56.00	−147.00	0	6.00 M_{PAS}	−54.03	−147.91	14:42:33.7	17	2.39
14 July (195) 1951	6:21:14.0	−52.00	−128.00	0		−53.05	−126.51	6:21:20.3	9	1.84

(*continued on next page*)

Table 1 (*continued*)

Date	Original (bulletin) location					Result of relocation				
Day Month (J) Year	Time (GMT)	Epicenter (°N)	(°E)	Depth (km)	Magnitude	Epicenter (°N)	(°E)	Time (GMT)	NS	σ (s)
Historical event relocating as outlier										
3 July (184) 1958	10:23:2.0	−55.00	−126.00	0		−54.84	−124.84	10:23:2.3	12	4.18
Historical events which could not be relocated										
20 July (202) 1920	0:21:35.0	−50.00	−127.00	0						
4 August (216) 1929	22:16:33.0	−55.00	−124.00	0						
26 January (026) 1952	14:2:54.0	−56.00	−146.00	0						
12 July (194) 1956	16:55:54.0	−58.00	−143.00	0						
6 February (037) 1961	11:25:38.9	−55.40	−130.60	25						

ments the offsets between TF 6 and the Tharp TF at 135°W, and between the Tharp and Heezen TFs at 127°W. Also, at the Eastern end of the Heezen TF, there is some suggestion of an offset to the north, defined by the three easternmost EHB events. Consequently, we targeted them for relocation, together

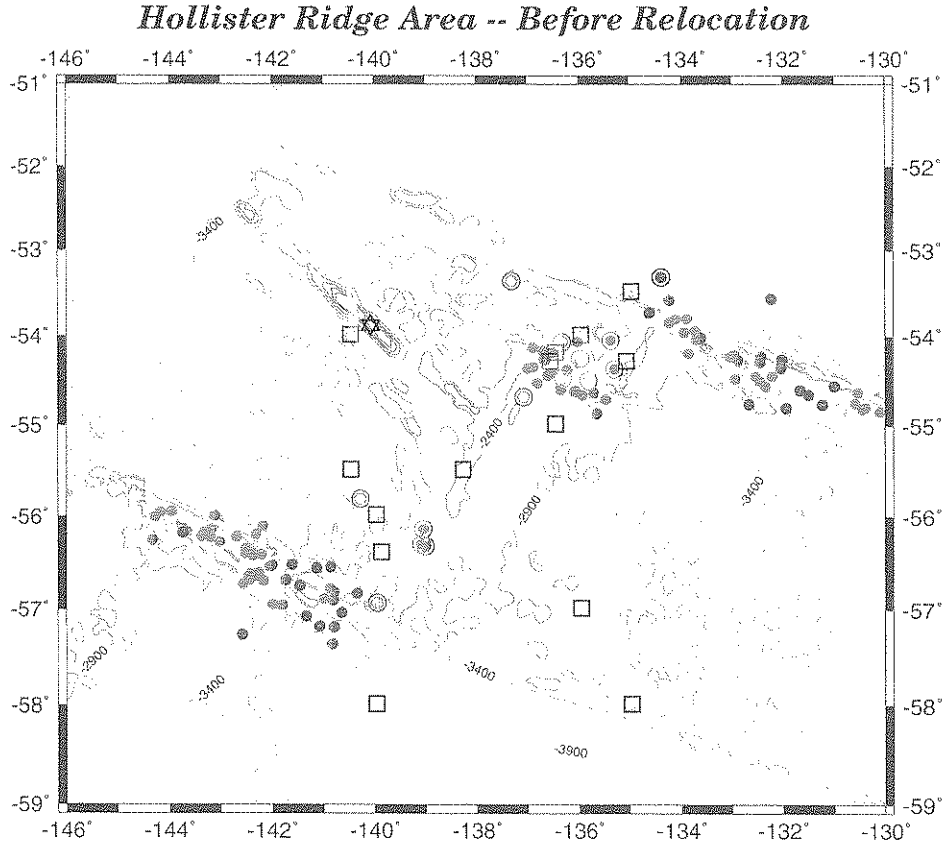

Fig. 3. Close-up of bulletin seismicity in the Hollister Ridge area. Symbols as in Fig. 1. Note scattered seismicity along PAR segment, and historical earthquake (open square) on the Hollister Ridge, in the immediate vicinity of the zone of acoustic activity in 1991 (Star of David). Isobaths after Smith and Sandwell (1995) at 500 m intervals from 900 to 3400 m.

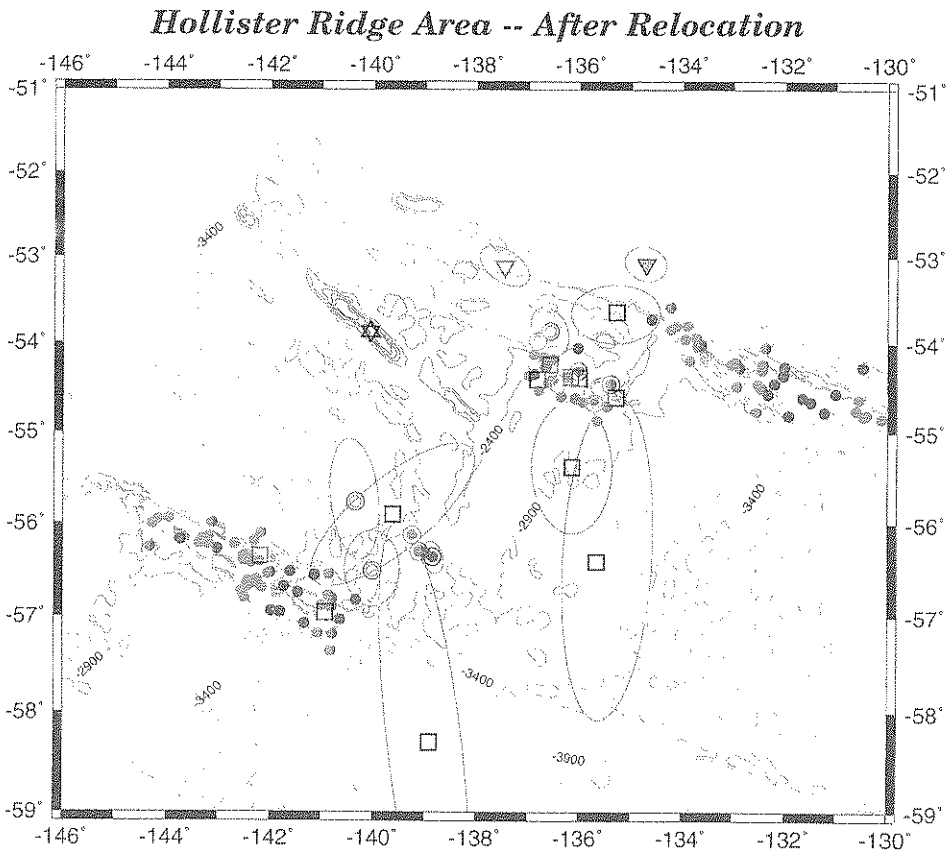

Fig. 4. Seismicity of Hollister Ridge area after relocation. Symbols as in Fig. 2. Note that the PAR segment and the Hollister Ridge are now aseismic.

with two modern, non-EHB earthquakes further West. These five solutions are listed as a special section of Table 1. The three EHB earthquakes are very well constrained, and two of them (12 November 1965 and 14 August 1980) have Monte Carlo ellipses which confirm a lateral offset of about 30 km to the Northeast, relative to the bulk of Heezen seismicity. The third event (09 April 1995) is most probably offset, but remains debatable. We thus propose that these three EHB earthquakes define a further offset in the Eltanin system, aligning on a 60-km-long transform, which we will call "TF 5 1/2". To the West, one of the non-EHB events (8 September 1995; 01:00) relocates on the inactive segment of TF 5 1/2; it could be described as an outlier event, but its Monte Carlo ellipse is too large for a definitive conclusion. The fifth event (8 May 1965) is poorly constrained, and could belong to the Heezen cluster to the Southwest.

An important aspect of the identification of TF 5 1/2 is that the four outlier events of 16 August 1984, 26 July 1987, 9 October 1966, and 3 July 1958, all lie in the immediate vicinity of the prolongation of FZ 5 1/2 outside of its active segment. As we progress further west, the outlier of 19 April 1993 at 129.5°W could lie on the inactive portion of the Heezen FZ, or on FZ 5 1/2.

In the Hollister region, the two outliers of 28 March 1982 and 26 June 1971 also lie on inactive segments of FZs, the former on the Heezen FZ, the latter on the Tharp FZ, to the north of the TFs active at the relevant longitudes, the Tharp FZ for the

Table 2
Relocation of Hollister region dataset
Note that all relocations were carried out at a constrained depth of 10 km; NS is the number of stations used in the relocation, σ the resulting root-mean-squared residual. An event is listed as "relocating to the TF system" if its Monte Carlo ellipse intersects at least one TF segment.

Date	Original (bulletin) location					Result of relocation				
Day Month (J) Year	Time (GMT)	Epicenter (°N)	(°E)	Depth (km)	Magnitude	Epicenter (°N)	(°E)	Time (GMT)	NS	σ (s)
Targeted EHB events relocating to TF systems										
19 September (262) 1965	13:55:39.0	−54.37	−135.30	10	4.8 m_b	−54.46	−135.39	13:55:37.7	21	2.26
23 December (357) 1973	18:31:30.3	−56.13	−139.05	10	5.7 M_s	−56.23	−139.22	18:31:29.6	15	2.52
19 April (109) 1981	10:10:49.8	−54.04	−135.37	12	5.1 M_s	−54.31	−136.02	10:10:50.8	9	2.74
16 May (136) 1989	17:22:54.2	−56.30	−139.09	10	5.8 M_s	−56.30	−139.12	17:22:53.5	39	1.32
21 October (294) 1993	7:36:57.2	−56.32	−139.01	11	5.6 M_w	−56.36	−138.85	7:36:56.5	27	1.67
Targeted EHB event relocating as outlier										
28 March (087) 1982	17:6:11.1	−53.31	−134.39	10	4.8 m_b	−53.08	−134.72	17:6:8.9	14	1.94
Modern, non-EHB, events relocating on TF systems										
26 May (146) 1967	9:14:39.7	−54.47	−136.31	33	4.9 m_b	−54.45	−136.44	9:14:37.6	16	2.31
3 May (124) 1968	20:9:24.0	−54.50	−135.82	33	4.2 m_b	−54.67	−135.71	20:9:23.6	11	2.68
21 September (264) 1969	20:48:9.0	−56.93	−139.95	33	4.5 m_b	−56.51	−140.02	20:48:6.3	10	3.96
28 August (240) 1974	23:6:28.4	−54.68	−137.07	33	4.6 m_b	−53.97	−136.82	23:6:27.4	12	3.31
26 May (147) 1984	5:38:26.4	−54.06	−136.34	10	5.0 m_b	−53.86	−136.58	5:38:26.2	15	1.37
31 May (151) 1985	20:16:34.7	−54.24	−135.98	10	4.8 m_b	−54.49	−135.61	20:16:37.4	9	2.73
4 October (277) 1995	15:30:3.3	−55.80	−140.27	10	4.3 m_b	−55.76	−140.35	15:30:4.5	7	0.58
Modern, non-EHB, event relocating as outlier										
26 June (177) 1971	18:12:32.4	−53.36	−137.30	33	5.1 m_b	−53.11	−137.47	18:12:29.2	10	0.32
Historical events relocating on TF system										
2 August (214) 1930	16:6:9.0	−58.00	−135.00	0		−56.46	−135.43	16:6:2.2	9	2.50
10 March (070) 1932	5:17:52.0	−54.30	−135.10	0		−54.63	−135.33	5:17:49.3	13	3.87
6 June (157) 1934	3:18:34.0	−56.00	−140.00	0	6.25 M_{PAS}	−58.32	−138.95	3:18:34.2	9	2.43
23 January (023) 1951	6:52:41.0	−55.00	−136.50	0	6.88 M_{PAS}	−55.29	−135.96	6:52:42.7	22	3.02
15 April (105) 1959	4:59:14.0	−53.50	−135.00	0		−53.66	−135.32	4:59:14.7	7	1.68
9 November (313) 1959	4:18:53.0	−57.00	−136.00	0		−54.43	−136.87	4:18:58.1	14	3.94
22 November (326) 1959	16:26:34.0	−54.00	−136.00	0		−54.41	−136.04	16:26:38.0	16	2.25
14 September (257) 1961	18:31:17.8	−56.40	−139.90	25		−55.91	−139.66	18:31:16.0	6	2.02
6 May (126) 1962	3:13:49.3	−54.30	−136.60	23		−54.26	−136.62	3:13:49.7	13	1.33
6 May (126) 1962	3:33:47.0	−54.20	−136.50	25		−54.40	−136.21	3:33:45.9	18	3.52
22 May (142) 1962	4:40:14.4	−55.50	−138.30	42		−56.98	−140.97	4:40:26.5	11	3.46
15 September (258) 1963	4:22:3.3	−55.50	−140.50	33	4.4 m_b	−56.37	−142.24	4:22:8.8	9	3.27
Historical event with blatant clerical error										
11 July (193) 1960	7:33:32.0	−54.00	−140.50	0		−54.10	140.63	7:33:33.5	12	0.65
Historical event which could not be relocated										
20 July (201) 1954	1:50:48.0	−58.00	−140.00	0						

former, TF 6 for the latter. It is remarkable than all seven outliers occur to the north of the active systems, none to the south.

The existence of a number of outlier earthquakes was pointed out by Lonsdale (1994), who noted that they occurred systematically to the north of the

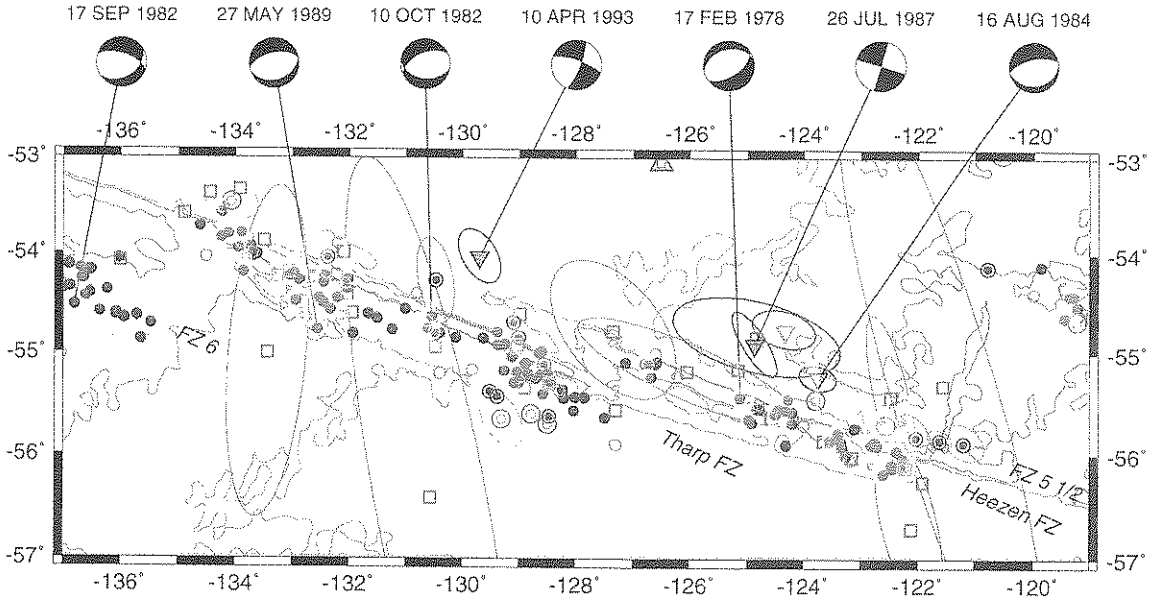

Fig. 5. Close-up of Fig. 2 in the central portion of the study area. Symbols as in Fig. 2. The Monte Carlo ellipses of the "outlier" events (shown as inverted triangles) are shown in dark. The three EHB events defining TF 5 1/2 are shown as bull's eye symbols at the eastern extremity of the Heezen system, together with their Monte Carlo ellipses. Also shown are seven CMT solutions: the five normal faulting events in this area, and the additional two solutions available for outlier events.

respective transforms, under a proposed regime of stress partitioning resulting from the Neogene reorientation. A more detailed discussion of this model will follow the examination of focal solutions.

3. Centroid moment tensor (CMT) solutions

There are 99 CMT solutions reported for the period 1977–1997 by the Harvard CMT project (Dziewonski et al., 1982 and subsequent quarterly updates) in the region under study. Of those, 91 have a strike–slip geometry (i.e., a null axis dipping more than 45°), and the remaining eight feature normal faulting. South of the region of interest, the PAR features an additional 28 solutions, 26 of which have strike–slip mechanisms, one a pure vertical dip–slip, and one a thrust geometry. These results are summarized in Fig. 6; they update to 1997 the dataset of anomalous earthquakes documented by Wolfe et al. (1993).

3.1. Anomalous geometries

The 1989 dip–slip event outside our region of study is located on the non-transform segment of FZ 9 1/2, as defined by Cande et al. (1995), on the eastern arm of the large V-shaped structure interpreted by Géli et al. (1997) as the wake of the spreading reorientation. The southernmost normal faulting solution (23 November 1985) is the intraplate earthquake shown as a triangle in Fig. 2, and occurring northeast of the active segment of TF8.

The remaining seven normal faulting earthquakes feature remarkably consistent mechanisms. Six of them occur on the Heezen, Tharp and Number 6 transforms, the seventh one on the Menard TF. It should be noted that three solutions (the 1982 and 1985 earthquakes) have very low moments of only 6.2×10^{23}, 6.5×10^{23} and 6.7×10^{23} dyn cm, below the threshold of completeness of the Harvard catalogue, generally taken as 10^{24} dyn cm. This raises the legitimate question of the reliability of such solutions, in particular given the remoteness of the epicenters. However, we note first that the CMT catalogue contains five Eltanin–Udintsev strike–slip solutions with moments below 10^{24} dyn cm, and also that the 1989 and 1995 events in Fig. 6 have both normal faulting solutions and much larger moments (respectively, 1.5×10^{25} and 2.7×10^{25} dyn

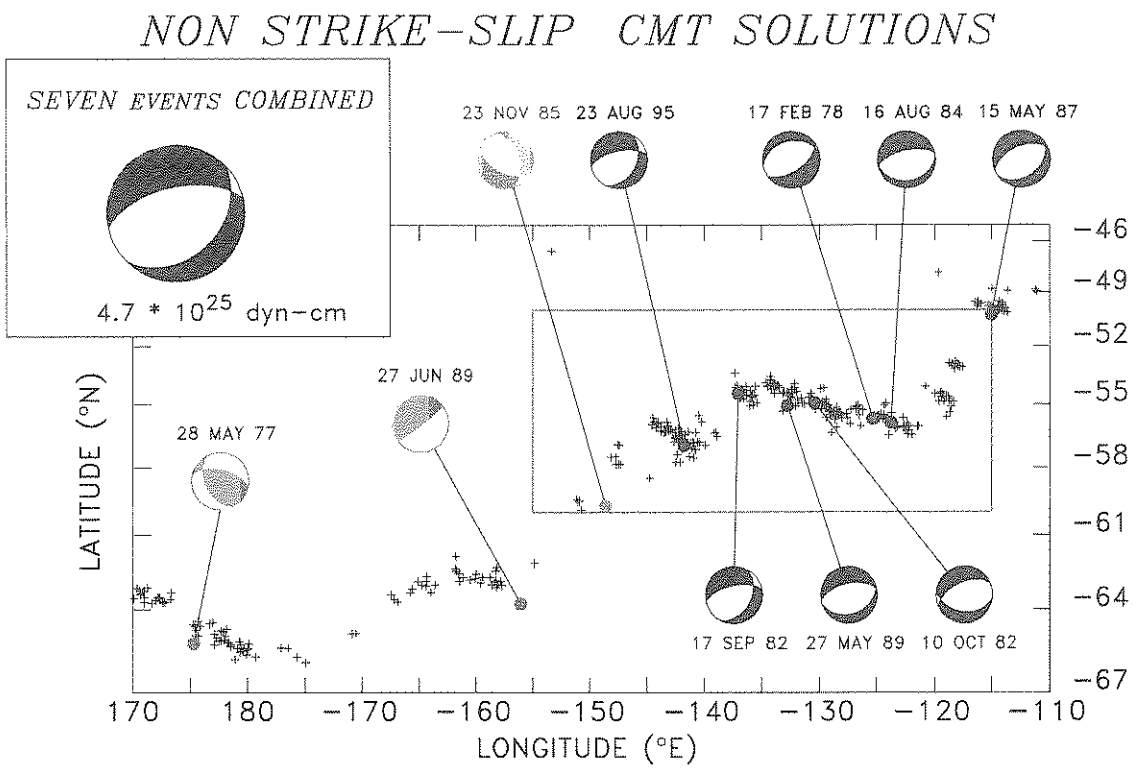

Fig. 6. Non-strike–slip CMT solutions in the study area (black beachballs), and further south along the PAR (gray symbols). The background seismicity is shown by the individual + signs (unrelocated, as available from the NEIC catalogue, 1964–1997). The gray box delineates the study area shown on Figs. 1 and 2.

cm); this argues against the small normal faulting solutions being possibly the result of a systematic error of the CMT algorithm for very small earthquakes. Also, Wolfe et al. (1993) conducted individual waveform inversions for two events, and examined first motion polarities on short-period seismograms from two smaller ones, thus confirming their non-strike–slip character. However, their solution for the earthquake of 17 February 1978 ($M_0 = 2.3 \times 10^{24}$ dyn cm) is significantly rotated from the published CMT; the origin of this discrepancy is unclear.

We further quantify the similarity of the normal faulting CMT mechanisms by adding the seven relevant moment tensors, and computing the double-couple best fitting the sum, shown in the inset of Fig. 6. The angular distances between that geometry and the seven individual solutions, as defined by Kagan (1991), range from 10° to 32°, with the larger distances applicable to the events with the smallest moments. This remarkable consistency between the non-strike–slip mechanisms suggests that they express the release of a coherent component of stress, present throughout the region under study. We note that the tensional axis of the best-fitting mechanism is sub-horizontal in the azimuth N26°W, and thus represents extension across the Eltanin system.

This systematic occurrence of normal faulting along transform segments of the Menard–Eltanin–Udintsev systems is unique as demonstrated by a comparison with other segments of the East Pacific Rise. Fig. 7 shows all CMT solutions with either predominant thrust or normal faulting (defined, respectively, as having their *T*- or *P*-axes steeper than 45°) along the East Pacific Rise, north of the region under study. Apart from clearly intraplate earthquakes, these anomalous mechanisms are found exclusively around the Easter and Juan Fernandez

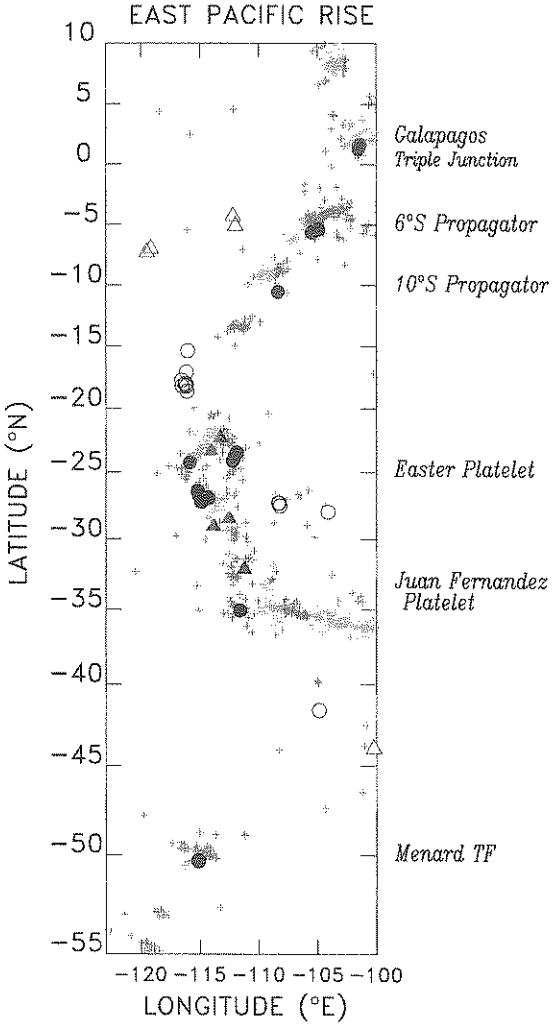

Fig. 7. Non-strike–slip focal solutions along the East Pacific Rise system, north of the study area. Background seismicity is shown in gray, based on the NEIC catalogue for 1964–1997. The large symbols show all available CMT solutions which are predominantly normal faulting (circles) or thrust faulting (triangles). Open symbols are intraplate events; solid ones are located on plate boundaries.

platelets, at the Galápagos triple junction, and at the tip of documented propagators, around 6°S and 10°S. None takes place along regular TF segments. Neither could we find a comparable pattern of normal faulting seismicity along the transform segments of the Romanche FZ in the Equatorial Atlantic, which may be comparable to the Eltanin system in terms of its total offset length: it is noteworthy that Wolfe et al. (1993) document in that region only a few thrust earthquakes, and one strike–slip mechanism rotated from its expected geometry, but no normal faulting solutions.

Lonsdale (1994) has proposed that both the location of the outlier events and the existence of normal faulting solutions could be ascribed to a pattern of stress partitioning following a reorientation of the Pacific–Antarctic motion at 5.9 Ma (Cande et al., 1995). In his model, the direction of spreading is maintained along the (old) Heezen Transform, and the spreading component taken up by the outliers in the marginal rifts to the north. In order to investigate this model further, we show in Fig. 5 the five normal faulting mechanisms in the central part of the Eltanin system, as well as two strike–slip CMT solutions for outlier events. Forty-eight more solutions (all left lateral strike–slip along the trend of the system) are available in that area; adding them to Fig. 5 would only clutter the plot.

We find no consistent correlation between normal faulting events and outliers: of the three outlier events with published CMT solutions, only one (16 August 1982) features normal faulting; the other two (26 July 1987 and 10 April 1993) have regular strike–slip geometries. Conversely, at least three normal faulting earthquakes (17 February 1978, 10 October 1982 and 17 September 1982) locate in the center of the Heezen, Tharp and Number 6 Transforms. We thus conclude that the populations of outlier and normal faulting events do not coincide as would be predicted by the model of Lonsdale (1994). Also, the normal faulting events on the transforms are not readily associated with lateral heterogeneities, such as a ridge–segment intersection, in the framework of the models of Engeln et al. (1986) and Huang et al. (1986).

Rather, the existence of strike–slip outlier events may suggest a pattern of ongoing evolution of the transforms in the study area, possibly involving lateral jumps of the short ridge segments connecting the large TFs (5 1/2, Heezen, Tharp, 6); e.g., Molnar et al. (1975) discuss some evidence for a westward migration of the Tharp-to-TF 6 segment between 8 and 3 Ma. If a similar pattern continued to this day, it could support the concept of two parallel segments of TFs being active at the same time. Any such model remains, however, highly speculative

given the ancillary nature of the outlier events, which are not expected to contribute significantly to any budget of the moment release in the area.

3.2. Compensated linear vector dipole (CLVD) components

We examine here the question of any possible systematic deviation of Eltanin earthquakes from pure double-couples, as measured by the "CLVD" parameter:

$$\varepsilon = \frac{-\sigma_2}{\max\left[|\sigma_1|,|\sigma_3|\right]} = \frac{\sigma_1+\sigma_3}{\max\left[\sigma_1,-\sigma_3\right]}, \qquad (1)$$

computed from the set of principal values of the stress release tensor ($\sigma_1 > \sigma_2 > \sigma_3$) published as part of the Harvard CMT solutions. Non-zero values of ε have been documented for earthquakes involving volcanic processes (e.g., Ekström, 1994).

The average value in our study area, $\langle \varepsilon \rangle = 0.016$, is not significant given the average absolute value $\langle |\varepsilon| \rangle = 0.10$; these results are comparable to those for the entire CMT catalogue of shallow earthquakes ($\langle \varepsilon \rangle = -0.002$, but $\langle |\varepsilon| \rangle = 0.12$). The earthquake with the largest CLVD component ($\varepsilon = 0.32$) is the normal faulting event on the Menard TF (15 May 1987; $M_0 = 2.1 \times 10^{24}$ dyn cm). This value is high, and would characterize the earthquake as a non-double-couple event. It should be kept in mind, however, that 274 shallow CMT solutions worldwide have a larger value of ε; they are spread around the plate boundary system and do not readily correlate with identifiably singular regions. Additionally, while the 1995 normal faulting earthquake on the Udintsev TF has a high ε (0.26), the five Heezen and Tharp normal faulting solutions have negligible CLVDs ($|\varepsilon| \leq 0.10$). In other words, the Eltanin–Udintsev earthquakes do not exhibit any anomalous behavior of their CLVD components.

4. Moment deficiency

In this section, we use the CMT database to reassess the seismic budget along the Eltanin FZ, in what amounts to an update of the calculation of Stewart and Okal (1983), which consisted of comparing the rate of seismic moment release on the Eltanin transforms to that expected from plate kinematic models. These authors, writing before the inception of the Harvard CMT project, had to interpret magnitude measurements in terms of seismic moments. Specifically, they used published M_s, or a variety of reported magnitudes for historical events, as representative of M_w; in doing so, they could, at least conceptually, have run the risk of underestimating the moment release rate, if the earthquakes had systematically featured large low-frequency components to their sources. The CMT catalogue now allows direct use of the seismic moment over the 21 years presently available.

In Table 3, we compile the total seismic moment release for all CMT solutions on five TFs of the study area. We then compare these figures to the moment release expected from the plate motion model NUVEL-1 (DeMets et al., 1990), using the following procedure: for each TF of length l, we

Table 3
Predicted and observed rates of moment release in the study area

TF	Length l (km)	Full rate v (cm/year)	Contact area A (km^2)	Moment release rate $\dot{M}_0$ (10^{26} dyn cm/year)		Percentage observed
				Predicted	Observed	
Udintsev	325	7.92	3500	8.4	0.65	7.7
TF 6	120	8.27	770	1.9	0.47	25
Tharp	520	8.36	6900	17.4	0.97	5.6
Heezen	350	8.41	3800	9.7	1.23	13
TF 5 1/2	60	8.45	270	0.7	0.039	6
Whole system	1375		15,240	38.1	3.36	8.8

compute the area of contact A between the two walls as:

$$A = \frac{2}{3} C \frac{l^{3/2}}{\nu^{1/2}}, \quad (2)$$

where $C = 8$ km/Ma$^{1/2}$ is the constant characterizing the thickening of seismogenic lithosphere with age (Stein, 1978). We then obtain the expected rate of moment release along the transform as:

$$\dot{M}_0 = \mu \nu A = \frac{2}{3} \mu C (l^3 \nu)^{1/2}, \quad (3)$$

where ν is the full spreading rate and $\mu = 3 \times 10^{11}$ dyn/cm^2, the rigidity of the shallowest part of the lithosphere.

Our expected values of $\dot{M}_0$ are generally lower than the estimates of Stewart and Okal (1983), because we have refined our geometrical description of the Eltanin system, principally by separating TF 6; we also use slightly lower values of the spreading rate. Nevertheless, the deficiency in actual seismic moment release remains close to 90% across the entire study area, with the exception of TF 6, where it reaches only 75%. Thus, we confirm that the general conclusion from Stewart and Okal (1983), namely that the moment release observed along the Eltanin transforms is one order of magnitude below that expected from kinematic models, is upheld by the use of a modern, homogeneous database of moment tensor solutions.

5. Frequency–size statistics

In this section, we investigate the distribution of Eltanin–Udintsev earthquakes with size, characterized through its β-value (Molnar, 1979), which describes the number N of earthquakes with moment greater than M_0 as:

$$\log_{10} N = \alpha - \beta \log_{10} M_0. \quad (4)$$

This parameter, introduced by Molnar (1979), is expected to take the value $2/3$ in the absence of any factor limiting the growth of source size on a two-dimensional fault (Rundle, 1989). We are motivated by the classical observation that β expresses the fractal dimension and the overall shape of the seismogenic material involved (see Frohlich and Davis, 1993; Romanowicz and Rundle, 1993 for a review). In particular, β is expected to take larger values in materials heavily fractured on a small scale, such as active volcanic structures, or upon delocalization of the seismogenic zone over a three-dimensional region (Okal and Kirby, 1995).

A regression of the dataset of 91 strike–slip CMT solutions in the Eltanin–Udintsev area yields $\beta = 1.08$; note in Fig. 8 that the dataset is well fit by a single straight line, but the absence of moments larger than 5.3×10^{25} dyn cm would suggest the initiation of fault saturation at that threshold, which in turn would correspond to a fault depth of 10 km (Okal and Romanowicz, 1994). When these results are compared with those from various other TF systems, we find a tentative inverse correlation between spreading rates and β-values in the non-saturated domain, with only the slowest-spreading transforms exhibiting the expected $\beta = 2/3$ (Langenhorst and Okal, 1999). The Eltanin–Udintsev result falls between the faster Northern segment of the East Pacific Rise ($\beta = 1.38$) and the slower-spreading Chile Rise ($\beta = 0.88$). Similarly, we note an apparent inverse correlation between the spreading rate and the saturation moment at which the slope β increases. If we interpret the maximum CMT moment of 5.3×10^{25} dyn cm as the saturation moment, our study area also falls between the Northern EPR (1.6×10^{25} dyn cm) and the Chile Rise (6.3×10^{25} dyn cm), but is singular in that the CMT dataset has no solutions beyond the saturation threshold.

In conclusion, the β-value for the Eltanin–Udintsev area is not anomalous among other oceanic transforms. There remains the puzzling observation that no earthquake larger than 5.3×10^{25} dyn cm has been recorded over the past 22 years. There is, however, some suggestion that larger historical events may have taken place (e.g., 3 September 1944; $M_{PAS} = 7.0$; $M_s = 6.9$ as measured by Stewart and Okal, 1983).

6. Energy–moment ratios and possible source slowness

We investigate in this section the ratio E/M_0 of the energy E radiated into an event's body waves to

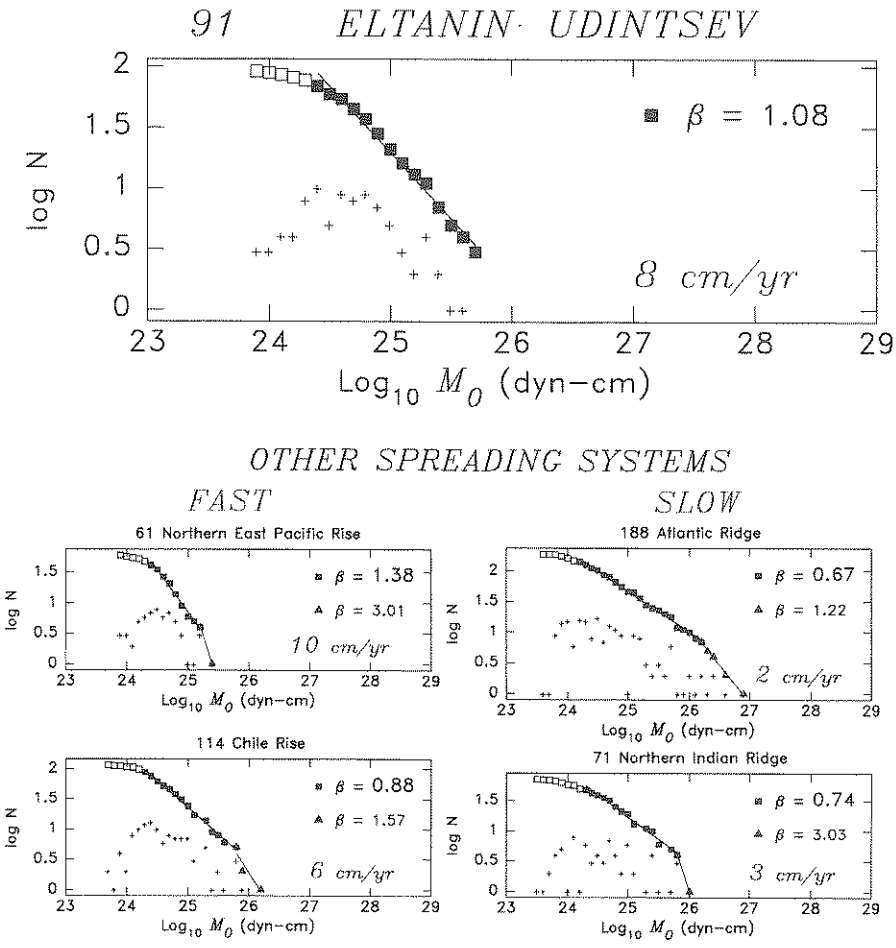

Fig. 8. Top: Frequency–moment relationship for 91 strike–slip CMT solutions in the study area. The + signs are the individual populations in bins of width 0.1 unit of $\log_{10} M_0$. The larger symbols are the cumulative values. The open squares correspond to the onset of incompleteness and are not used in the regression. Bottom: Same as top for other geographical areas along the MOR system. In those instances, and because of a clear break in the relationship upon the onset of saturation, two separate regressions were performed: main population (squares) and large events (triangles). The (average) full rates of spreading of the five systems are also shown.

its seismic moment M_0, following the technique described in detail by Newman and Okal (1998). Any earthquake featuring a parameter $\Theta = \log_{10} E/M_0$ significantly less than the expected theoretical value of -4.90 features a source process preferably exciting low-frequency spectral components, and thus corresponding to a slow propagation of the rupture along the fault plane; in particular, Newman and Okal showed that the discriminant Θ readily identifies the so-called ''tsunami earthquakes''. By analogy with such cases, we explore the possibility of source slowness along the Eltanin transforms. Should it be detected, it might explain at least partially the moment deficiency by suggesting either a hidden moment component at periods longer than used in the Harvard CMT inversion, or the presence of sedimentary or otherwise mechanically deficient structures along the fault walls.

Fig. 9 shows energy E as a function of moment M_0 for 20 events, which we were able to process among available CMT solutions for the Eltanin–Udintsev region. These are shown as dark symbols, with the dataset of Newman and Okal (1998) shown as background in half-tone. The average value of Θ

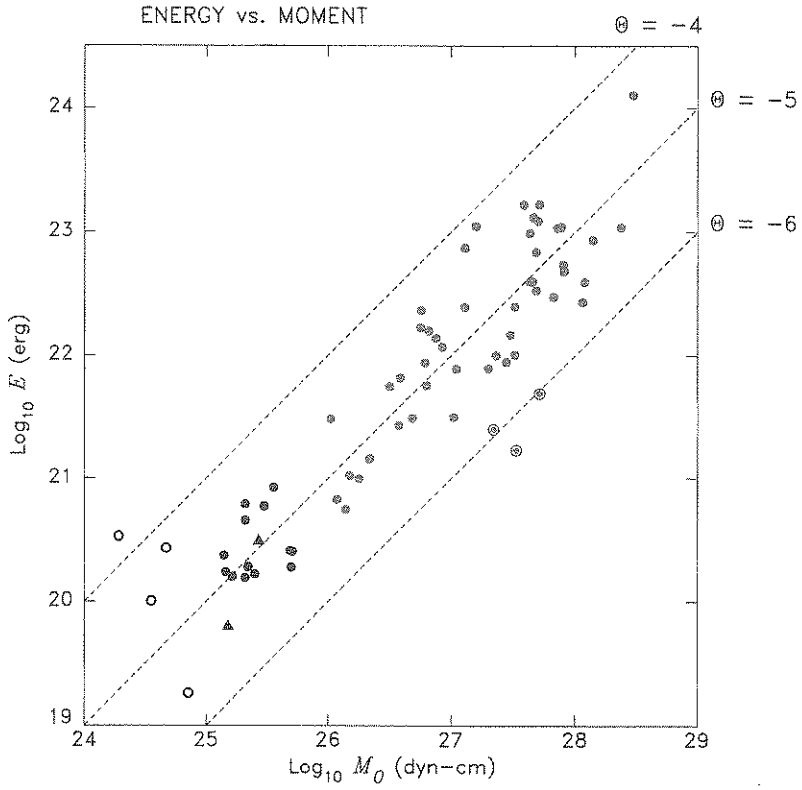

Fig. 9. Energy vs. moment diagram for 20 earthquakes in the Eltanin–Udintsev system (dark symbols). The open circles represent smaller events, below 10^{25} dyn cm, for which the computation of E may be affected by noise. The two triangles show solutions with normal faulting mechanisms. The 54 half-tones symbols are the dataset of Newman and Okal (1998), and are given for reference. Among them, the three bull's eye symbols identify the three "tsunami" earthquakes with strongly deficient values of $\Theta = \log_{10} E/M_0$. Note that the Eltanin–Udintsev events do not exhibit an anomalous behavior in terms of Θ.

in our study area is -4.90, and its lowest value, -5.59; however, note that the smaller events ($M_0 \leq 10^{25}$ dyn cm; shown as open circles) have scattered values of E/M_0; such moments are below the threshold of study by Newman and Okal (1998). If those four events are discarded, the average value of Θ is practically unchanged (-4.97), and its lowest value slightly increased (to -5.41). Finally, the two events in the dataset with normal faulting mechanisms (solid triangles) do not stand out with singular values of Θ.

We conclude that no earthquakes along the Eltanin–Udintsev system could be found to exhibit the strong deficiency of 1–1.5 units in Θ characteristic of the slower earthquakes in subduction zones (shown on Fig. 9 as bull's eye symbols as part of the background data). A further comparison with earthquakes along both the Romanche FZ in the Atlantic, and the other transform systems farther South on the PAR, similarly failed to identify any resolvable difference in behavior. In this respect, the seismic moment deficiency along the Eltanin system cannot be ascribed to the presence of mechanically deficient material, which would result in anomalously slow velocities of rupture along the fault.

7. Plate kinematics models

In this section, we investigate to which extent the behavior of the Pacific plate in the Eltanin FZ area could be considered non-rigid. This hypothesis is

Table 4
Plate kinematic inversions
$\boldsymbol{\omega}_{PA-SP}$ is given by its pole and amplitude ω (in degrees per million years). In the convention used, a positive ω means that the second plate (SP) rotates counterclockwise with respect to the first plate (PA). σ_{max} (respectively, σ_{min}) is the length (in degrees) of the major (respectively, minor) axis of the 95% confidence ellipse of the pole of $\boldsymbol{\omega}$. ζ is the azimuth (in degrees, clockwise from north) of the major axis. σ_ω is the uncertainty on the amplitude ω.

Dataset	N	ν_1	ν_2	χ^2_{12}	χ^2_{13}	F	P (%)	$\boldsymbol{\omega}_{PA-SP}$ in 13-plate inversion						
								°N	°E	ω	σ_{max}	σ_{min}	ζ	σ_ω
NUVEL-1	1122	3	1086	261.739	260.295	2.008	89	−45.7	−160.5	0.08	49.1	26.4	9	0.14
XE	1099	3	1063	259.908	258.305	2.199	91	−38.9	−157.0	0.07	52.2	25.1	4	0.14
XEU	1088	3	1052	259.316	257.916	1.903	87	−43.1	−162.6	0.08	56.8	29.6	10	0.15
X5EU	1080	3	1044	255.317	254.160	1.584	81	−43.2	−164.0	0.08	56.3	29.6	9	0.15

legitimate in the presence of the massive Hollister volcanic structure, and also given the existence of the "V-shaped" propagator further South along the ridge (Géli et al., 1997), indicating that a more complex system of plate kinematics has been evolving for the past few million years (Cande et al., 1995), and could still be influencing the plates' motion. We conclude that the available data cannot resolve a lack of rigidity of the Pacific plate.

We address the problem by comparing inversions of the NUVEL-1 dataset (DeMets et al., 1990) involving different descriptions of the plate system in that part of the Pacific Basin. Since we wish to test the possibility of non-rigid behavior along the Eltanin and adjoining TFs, we consider several versions of the datasets: XE ("Except Eltanin"), in which we suppress all data (rates, azimuths of transforms and slip vectors) along the South Pacific Ridge between 139°W and 121°W; XEU ("Except Eltanin and Udintsev", with data neutralized between 147°W and 121°W); and X5EU ("Except TF 5, Eltanin, Udintsev", with data suppressed between 117°W and 147°W), as well as the full NUVEL-1 dataset. Each of these datasets is then inverted both in the regular 12-plate NUVEL-1 geometry, and in a hypothetical 13-plate model in which the Southwestern part of the Pacific plate West of 139°W (SP) is left free to move independently. Assuming, e.g., that the Eltanin TF system is leaking, one would expect a significant variance reduction when inverting Dataset XE with the 13-plate model. The 13-plate inversions should also yield a PA–SP rotation vector (South Pacific with respect to Main Pacific), which could be used to compute a relative motion, and hence a state of stress, at the boundary of the two plates, in the vicinity of the Hollister Ridge. Similarly, one could hope to study the nature (extensional or compressional) of the transverse component of motion across the Eltanin transform segments, where non-strike–slip focal mechanisms are observed (see Section 3).

Table 4 lists the results of all inversion experiments. Following Stein and Gordon (1984), we list the χ^2 residual parameters for inversions involving $p = 12$ and 13 plates, respectively, and interpret them in terms of the so-called F-parameter:

$$F = \frac{\frac{\nu_2}{\nu_1}\left[\chi^2_{12} - \chi^2_{13}\right]}{\chi^2_{13}}, \tag{5}$$

where N is the number of data points inverted, $\nu_2 = N - 3p$ is the number of degrees of freedom of the 13-plate inversion, and $\nu_1 = 3$ is the increase in ν_2 when using the 12-plate model. In turn, the probability P that the decrease in χ^2 is due to an intrinsically better model, rather than randomly attributable to the increase in the dimension of the model space, is given by the Snedecor distribution (e.g., Snedecor and Cochran, 1980):

$$P(F|\nu_1,\nu_2) = \frac{\nu_1^{\frac{\nu_1}{2}}\,\nu_2^{\frac{\nu_2}{2}}}{B\left(\frac{\nu_1}{2},\frac{\nu_2}{2}\right)}\int_0^F f^{\frac{\nu_1-2}{2}}\left(\nu_2+\nu_1 f\right)^{-\frac{\nu_1+\nu_2}{2}} df, \tag{6}$$

with $B(a,b) = \Gamma(a)\Gamma(b)/\Gamma(a+b)$. For large ν_2, it is possible to use the approximation:

$$P(F|\nu_1,\nu_2) \approx \frac{1}{2}\left[1 + \mathrm{erf}(\xi)\right]$$

$$\text{with} \quad \xi = \frac{\left(1 - \frac{2}{9\nu_2}\right)F^{1/3} - \left(1 - \frac{2}{9\nu_1}\right)}{2\left(\frac{1}{9\nu_1} + \frac{F^{2/3}}{9\nu_2}\right)^{1/2}} \qquad (7)$$

(Abramowitz and Stegun, 1972), which makes it straightforward to assess the significance of F. Table 4 shows that, although the values of P remain high (up to 91%), they fall short of the threshold of 95% generally regarded as an absolute minimum for confidence, and we must conclude that the F-tests fail to assert the 13-plate model as a better fit to the existing datasets.

In addition, Table 4 shows that the uncertainties in the relative rotation vector $\boldsymbol{\omega}_{\mathrm{PA-SP}}$ are of such magnitude as to invalidate its use for any tectonic interpretation; e.g., $\sigma_\omega > |\boldsymbol{\omega}|$, meaning that a 13-plate inversion cannot even resolve the sense of rotation of SP with respect to PA.

We conclude that there is no evidence in the NUVEL-1 dataset to support any suggestion of either leakage across the Eltanin system, or non-rigid behavior of the Pacific plate.

8. Discussion and conclusion

In summary, we identify or confirm two anomalous properties in the Eltanin–Udintsev area. First, the seismic moment release, as compiled from published CMT solutions over the past 21 years, accounts for only 9% of the expected motion between the Pacific and Antarctic plates. This result, obtained from a homogeneous quantitative CMT database, upholds the study of Stewart and Okal (1983), which had to rely on the interpretation of various magnitude scales in terms of seismic moment. Second, normal faulting earthquakes are found to take place regularly on transform segments. The remarkable coherence in their mechanisms suggests that they truly express the release of an ambient tectonic stress even though they represent only a small fraction of the seismicity of the TFs, both in number of events (8% of published CMT solutions) and in total moment release (4%).

The second intriguing observation is the presence of seven outlier earthquakes on the supposedly inactive segments of the FZs, north of the plate boundary (we have not documented any on the Antarctic side). At least three of them feature strike–slip mechanisms, which rules out their interpretation as resulting from stress partitioning.

On the other hand, most other seismic properties along the Eltanin system are typical of a long TF on a fast-spreading mid-ocean plate boundary. The seismicity is confined to well-defined TFs, with no activity documented on the ridge segments linking them. There is no evidence for delocalization of the TF seismicity across a transversally broad region, which would have suggested a leaky transform. We could not relocate a single conventionally recorded earthquake on the Hollister Ridge. Eltanin earthquakes do not exhibit source slowness, but rather their energy-to-moment ratios are comparable to worldwide values. Some events do feature non-double-couple components, but their occurrence falls well within worldwide statistics. Frequency–size relations on the TFs of the Eltanin system are within the trends observed elsewhere on the Mid-Oceanic system. Finally, we examined the NUVEL-1 dataset, and could find no kinematic evidence suggesting non-rigid behavior of the Pacific plate in the vicinity of the Eltanin system.

Thus, and, to a large extent, this study fails to document characteristics of the seismicity of the Hollister and Eltanin areas which could be taken as direct evidence of either large-scale volcanic processes or clearly anomalous plate boundary patterns. In the case of the Hollister Ridge, the lack of teleseismic evidence of volcanic activity is not exceptional, given that a number of other submarine volcanoes in the Pacific (Macdonald, Mehetia, Teahitia) have remained silent for teleseismic receivers sampling the conventional seismic band, even though they underwent documented episodes of eruption in the past few decades (Johnson, 1970; Talandier and Okal, 1984a,b; Talandier et al., 1988). We note, however, that Loihi regularly features events detected teleseismically.

Regarding the seismicity of the Eltanin system, it would be tempting to try to interpret the occurrence of normal faulting earthquakes in the framework of the change of absolute motion of the Pacific plate which Wessel and Kroenke (1997) have proposed occurred at 4 Ma following the collision of the Ontong–Java Plateau with the Solomon Trench; they give a present pole location at 25°S and 153°E, and a rate of 1.19°/Ma. The effect of such a reorganization on the other lithospheric plates, and hence on relative plate motion vectors, is open to speculation, but one end member would be to assume that the Antarctic plate's absolute motion was unaffected. Fig. 10 shows that this model (''A'') predicts a velocity of 11.7 cm/year in the N5°W azimuth for the Pacific plate relative to Antarctica at a reference point located in the center of the Eltanin system (54°S; 130°W). The azimuth would indeed be in reasonable agreement with the geometry of the eight normal faulting events on Fig. 6, whose average T-axis is in the direction N26°W. It would, however, be hard to reconcile with the 91 other solutions, all of them strike–slip, all but the four on TF 4, left-lateral. Indeed, the total moment released through normal faulting in the Eltanin system over the lifetime of the CMT project (2.2×10^{25} dyn cm over 21 years) remains incidental when compared with its strike–slip counterpart (5.6×10^{26} dyn cm or 25 times more). Because, as discussed in Section 4, the latter is an order of magnitude less than predicted, one could, under Model A, reverse the argument, and regard the strike–slip events as incidental to the plate motion, with most displacements taking place aseismically along what should be fast-opening (11.7

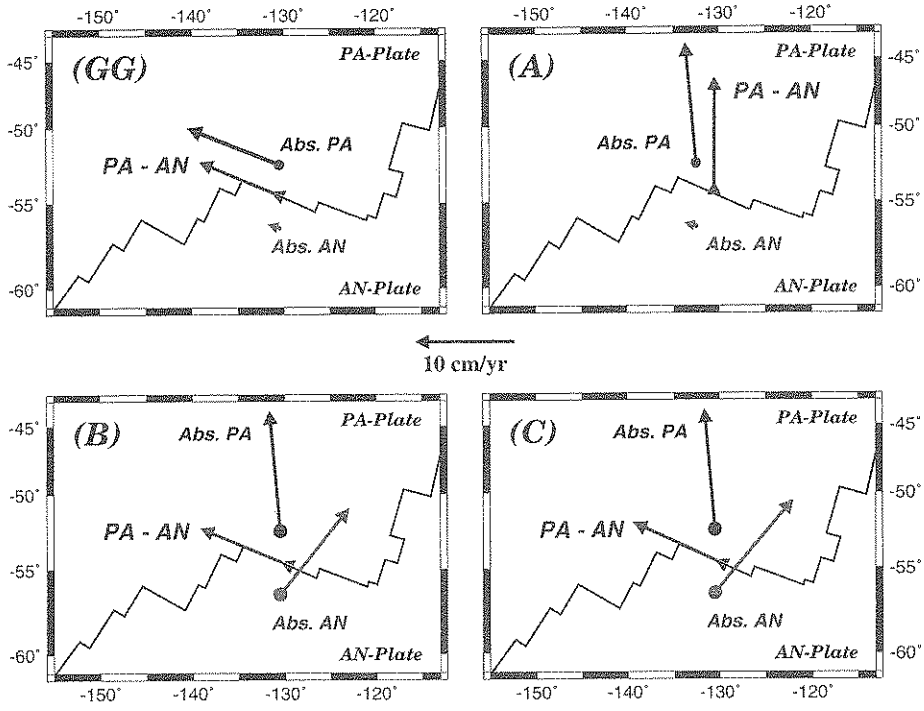

Fig. 10. Cartoons illustrating various possible plate motions in the Eltanin area. The jagged line is the Pacific–Antarctic plate boundary. On each plate, the absolute motions of the two plates are shown, as well as the relative motion of the Pacific plate with respect to Antarctica (labeled ''PA–AN''). All vectors are computed for a point at 54°S; 140°W, in the center of the Eltanin system; however, the absolute vectors have been displaced in the interior of the plates to reduce clutter. (GG): Plate motions in the absolute model HS2–NUVEL-1 by Gripp and Gordon (1990). (A): Plate motions combining the present absolute pole for the Pacific plate of Wessel and Kroenke (1997), with the HS2–NUVEL-1 absolute pole for Antarctica. (B): Plate motions combining the absolute pole of Wessel and Kroenke for the Pacific plate and the NUVEL-1 PA–AN relative pole. (C): Same as (B), but allowing a small amount of extension across the Eltanin system. See text for details.

cm/year) spreading segments. This is, however, totally incompatible with the dataset of magnetic anomalies younger than 4 Ma (Chrons 1 and 2) in the region (e.g., Molnar et al., 1975). Finally, under Model A, the lone left-offset transform, TF 4, should be submitted to convergence at more than 10 cm/year, whereas all four available CMT solutions on TF 4 are right-lateral strike–slip.

The other end member model (''B'' on Fig. 10) would assume that the relative PA–AN motion was unchanged during the reorientation, which of course would predict the correct strike–slip solutions. However, this would require an absolute rotation of Antarctica at 0.97°/Ma, about a pole at 22°N, 174°E, which would in turn move Erebus over the mantle at 9.5 cm/year in a north–south direction (or 380 km since the reorientation), for which we do not know of any field evidence, not to mention similar difficulties inside other plates, propagated through closure relations at other boundary systems. We also tried to build an ad hoc kinematic model (''C''), in which we define a direction of relative motion between the two plates PA and SP by combining the slip vector of the strike–slip events, with the *T*-axis of the normal solutions, weighted by the relevant total seismic moment released over the duration of the CMT catalogue: the result is a PA–AN vector pointing N110.8°E, only 1.2° away from the mean slip in the strike–slip events (N109.6°E). In this respect, Model C is fundamentally undistinguishable from B, and therefore faces the same unsurmountable problems.

We conclude that, despite the intriguing character of the normal faulting events, the composite seismicity of the Eltanin system does not support the idea of a drastic change of absolute motion of the Pacific plate having taken place 4 Ma ago, with a new pattern of plate motions presently in effect, as advocated by Wessel and Kroenke (1997). The stresses released during the normal faulting events, together with the deficiency in moment release, would generally be compatible with extension across the Eltanin system, which could at best express a developing or incipient change in plate motions; however, the majority of the seismic characteristics of the region still fits a conventional model such as NUVEL-1. A satisfactory model for the origin of the two anomalous properties of the Eltanin system, namely its deficiency in moment release, and the presence of normal faulting earthquakes, may be sought in an examination of the state of stress of the two plates on either side of this exceptionally long transform system (Beutel et al., 1999).

Note added in proof: Since this work was completed and written-up, a further normal faulting event occurred, on 1 June 1999, on the center of the Heezen TF (124.0°W; $M_0 = 1.1 \times 10^{24}$ dyn cm).

Acknowledgements

We thank Seth Stein for a tutorial on the use of the NUVEL dataset and software, and Louis Géli for sending us detailed results of the cruise of *L'Atalante* in advance of publication. The paper was improved by comments from Göran Ekström and another reviewer. Many figures were drafted using the GMT software of Wessel and Smith (1991).

Appendix A. Details of relocations

A.1. Seismicity of the Eltanin transforms system

A.1.1. Events selected

The solid dots on Fig. 1 are the 211 EHB epicenters for the years 1964–1995 (Fig. 1). They generally define the transform segments well. However, 17 earthquakes, shown with larger bull's eye symbols, are in apparent violation of this trend and were selected for relocation.

The 55 open circles are additional events listed by the NEIC bulletins during the period of the EHB catalogue. They mostly represent smaller earthquakes ($m_b \leq 5.4$) which Engdahl et al. (1998) did not or could not relocate. Among them, 12 events (shown as two concentric circles) had bulletin locations lying outside the trends of the TFs, and were targeted for relocation.

The open squares represent 53 historical earthquakes (1920–1963) with bulletin locations in the study area. All were targeted for relocation.

A.1.2. Relocation results

Among the 17 EHB epicenters, 12 either relocated to the nearby transform, or had Monte Carlo ellipses (usually with $\sigma_G = 1$ s) intersecting it (Fig.

2). These are plotted as bull's eye symbols on Fig. 2. We confirm two earthquakes, shown as solid dots inscribed in triangles, as clearly intraplate: the event of 21 December 1987 (57.00°S, 149.67°W) locates on FZ 6, but 125 km northwest of its transform segment, and that on 23 November 1985 (59.67°S, 148.60°W) takes place northeast of FZ 8, again about 125 km from the nearest plate boundary seismicity. Finally, we define three EHB events as ''outliers'': these earthquakes relocate to the inactive section of a FZ, and are shown on Fig. 2 as shaded inverted triangles. The event on 10 April 1993 ($m_b = 4.7$) relocates at 54.04°S, 129.70°W, on the western extension of the Heezen FZ, in its supposedly inactive segment, about 65 km north of the Tharp seismicity, and slightly north of the EHB solution, which constitutes the southern limit of the Monte Carlo ellipse. The quality of this epicenter is excellent ($\sigma = 0.96$ s), and the ellipse ($\sigma_G = 1$ s) does not intersect the cluster of Tharp seismicity to the south. Similarly, but farther southeast, the two events of 16 August 1984 ($m_b = 5.3$) and 26 July 1987 ($m_b = 4.7$) relocate 40 km north of the Heezen active segment, which is not reached by their error ellipses (even with $\sigma_G = 2.0$ s). These two shocks cannot be assigned to the active TF segment.

Among the 12 modern NEIC events relocated, only three remain outside the immediate vicinity of the TF segments: The earthquake of 30 January 1993 ($m_b = 4.8$; $M_s = 5.3$) relocates at 56.33°S, 118.22°W, on the Heezen FZ, 200 km east of its transform segment, but is poorly constrained and its Monte Carlo ellipse intersects TF 5. On the other hand, the event of 9 December 1990 at 58.36°S, 144.84°W, is genuinely intraplate, 135 km east of the TF segment on FZ 6; this shock is shown in Fig. 2 as an open circle inscribed in a triangle. As for the earthquake of 9 October 1966, shown in Fig. 2 as an inverted open triangle, it relocates 60 km north of the active Heezen segment, in the general area of the 1987 EHB event described above, and also qualifies as an ''outlier''.

Among the historical earthquakes, two events were previously studied (Wysession et al., 1991) and determined to be intraplate (5 September 1938 and 14 July 1951); they are shown, with their Monte Carlo ellipses, as open squares inscribed in triangles; five more (20 July 1920, 4 August 1929, 26 January 1952, 12 July 1956, 6 February 1961) could not be reliably relocated. Of the remaining 46, only nine relocate to epicenters significantly removed from transform segments; in all cases but one, their Monte Carlo ellipses (shown on Fig. 2) intersect transforms, leaving only the event of 3 July 1958 as an ''outlier'', sharing its epicenter with the EHB event of 26 July 1987 described above.

A.2. Seismicity of the Hollister region

A.2.1. Events selected

The solid dots are the EHB epicenters for the period 1964–1995, of which six were targeted for relocation (bull's eye symbols): one at the western end of the Tharp active segment (28 March 1982), two events located between the Tharp and TF6 clusters (19 September 1965 and 19 April 1981), and the three events defining TF 7 (23 December 1973, 16 May 1989 and 21 October 1993) (Fig. 3). All eight additional NEIC events during 1964–1995 were also targeted (plotted as two concentric circles), as were all 14 historical events (squares).

A.2.2. Relocation results

Among EHB events, we confirm the location of the three earthquakes defining TF 7; the combination of very small Monte Carlo ellipses, and two CMT strike–slip solutions (16 May 1989; 21 October 1993) is irrefutable proof of the existence of this small transform offset; note in particular that the left-lateral character of these solutions (see Fig. 10 of Talandier and Okal, 1996) dictates that Transform 7 should have a right-lateral offset, rather than a left-lateral one, as suggested by Small (1995) (Fig. 4).

The two events with EHB locations between the Tharp transform and TF 6 relocate to TF 6. As for the event of 28 March 1982, we relocate it slightly to the northwest of its EHB epicenter, on the Heezen FZ; its small Monte Carlo ellipse does not intersect the Tharp cluster, and the event must be considered an ''outlier''. We show it as a shaded inverted triangle in Fig. 4.

Among modern NEIC epicenters, four events relocate to the TF 6 cluster, and a fifth one (28 August 1974) has a Monte Carlo ellipse which intersects the cluster. The ellipse for a sixth event (21 September

1969) reaches the Udintsev transform, and that for the small event of 4 October 1995 ($m_b = 4.3$) reaches TF 7. As for the last event (26 June 1971; $m_b = 5.1$), it relocates to the extension of the Tharp system, and its ellipse ($\sigma_G = 1.5$ s) remains 90 km away from the cluster on TF 6. We show this outlier event as an inverted open triangle in Fig. 4.

Seven older events relocate inside the Udintsev and TF 6 clusters. Four more have Monte Carlo ellipses intersecting one of the active TF segments. The earthquake of 14 September 1961 could be either on TF 7 or on the Udintsev transform. One event (20 July 1954, with only three South American times reported) could not be meaningfully relocated, and the last older event (11 July 1960), with a bulletin location on the Hollister Ridge, at the exact location of the 1991–1993 volcanic swarms (54°S, 140.5°W), involves a flagrant typographic error, since it relocates south of Australia, at 54.1°S, 140.6°E.

References

Abramowitz, M., Stegun, I., 1972. Handbook of Mathematical Functions. Dover, New York, 1046 pp.

Beutel, E.K., Okal, E.A., Langenhorst, A.R., Russo, R.M., 1999. Anomalous earthquakes along the Eltanin Transform: long equals strong?. Geol. Soc. Am. Abstr. Prog. 31 (7), A377, (Abstract).

Cande, S.C., Raymond, C.A., Stock, J., Haxby, W.F., 1995. Geophysics of the Pitman Fracture Zone and Pacific–Antarctic plate motions during the Cenozoic. Science 270, 947–953.

DeMets, D.C., Gordon, R.G., Argus, D.F., Stein, S., 1990. Current plate motions. Geophys. J. Int. 101, 425–478.

Dziewonski, A.M., Friedman, A., Giardini, D., Woodhouse, J.H., 1982. Global seismicity of 1982: centroid moment tensor solutions for 308 earthquakes. Phys. Earth Planet. Inter. 33, 76–90.

Ekström, G., 1994. Anomalous earthquakes on volcano ring-fault structures. Earth Planet. Sci. Lett. 128, 707–712.

Engdahl, E.R., van der Hilst, R., Buland, R.P., 1998. Global teleseismic earthquake relocation with improved travel times and procedures for depth determination. Bull. Seismol. Soc. Am. 88, 744–757.

Engeln, J.F., Wiens, D.A., Stein, S., 1986. Mechanisms and depths of Atlantic transform earthquakes. J. Geophys. Res. 91, 548–577.

Frohlich, C., Davis, S.D., 1993. Teleseismic b-values; or, much ado about 1.0. J. Geophys. Res. 98, 631–644.

Géli, L., Bougault, H., Aslanian, D., Briais, A., Dosso, L., Etoubleau, J., Le Formal, J.-P., Maia, M., Ondréas, H., Olivet, J.-L., Richardson, C., Sayanagi, K., Seama, N., Shah, A., Vlastelic, I., Yamamoto, M., 1997. Evolution of the Pacific–Antarctic Ridge south of the Udintsev fracture zone. Science 278, 1281–1284.

Gripp, A.E., Gordon, R.G., 1990. Current plate velocities relative to the hotspots incorporating the NUVEL-1 global plate motion model. Geophys. Res. Lett. 17, 1109–1112.

Gutenberg, B., Richter, C.F., 1954. Seismicity of the Earth and Associated Phenomena. Princeton Univ. Press.

Huang, P.Y., Solomon, S.C., Bergman, E.A., Nábělek, J.L., 1986. Focal depths and mechanisms of mid-Atlantic ridge earthquakes from body waveform inversion. J. Geophys. Res. 91, 579–598.

Johnson, R.H., 1970. Active submarine volcanism in the Austral Islands. Science 167, 977–979.

Kagan, Y.Y., 1991. 3D rotation of double-couple earthquake sources. Geophys. J. Int. 106, 709–716.

Kennett, B.L.N., Engdahl, E.R., 1991. Travel times for global earthquake locations and phase identification. Geophys. J. Int. 105, 429–465.

Langenhorst, A.R., Okal, E.A., 1999. The variation of β-values for strike–slip oceanic transform fault earthquakes. EOS, Trans. Am. Geophys. Union 80 (46), F651, (Abstract).

Lonsdale, P., 1994. Structural geomorphology of the Eltanin Fault system and adjacent transform faults of the Pacific–Antarctic plate boundary. Mar. Geophys. Res. 16, 105–143.

Molnar, P., 1979. Earthquake recurrence intervals and plate tectonics. Bull. Seismol. Soc. Am. 69, 115–133.

Molnar, P., Atwater, T., Mammerickx, J., Smith, S.M., 1975. Magnetic anomalies, bathymetry, and tectonic evolution of the Pacific since the Late Cretaceous. Geophys. J. R. Astron. Soc. 40, 383–420.

Natland, J.H., Castillo, P.R., Niu, Y., Bloomer, S.H., Lonsdale, P., 1995. Dredging exploration of fast-spreading ridges in the far Southern Pacific Ocean: a preliminary report. Ridge Events 6, pp. 1–2, 26–27.

Newman, A.V., Okal, E.A., 1998. Teleseismic estimates of radiated seismic energy: the E/M_0 discriminant for tsunami earthquakes. J. Geophys. Res. 103, 26885–26898.

Okal, E.A., 1984. Intraplate seismicity of the southern part of the Pacific plate. J. Geophys. Res. 89, 10053–10071.

Okal, E.A., Kirby, S.H., 1995. Frequency–moment distribution of deep earthquakes: implications for the seismogenic zone at the bottom of slabs. Phys. Earth Planet. Inter. 92, 169–187.

Okal, E.A., Romanowicz, B.A., 1994. On the variation of b-value with earthquake size. Phys. Earth Planet. Inter. 87, 55–76.

Romanowicz, B.A., Rundle, J.B., 1993. Scaling relations for large earthquakes. Bull. Seismol. Soc. Am. 83, 1294–1297.

Rundle, J.B., 1989. Derivation of the complete Gutenberg–Richter magnitude–frequency relation using the principle of scale invariance. J. Geophys. Res. 94, 12337–12342.

Small, C., 1995. Observations of ridge–hotspot interactions in the Southern Ocean. J. Geophys. Res. 100, 17931–17946.

Smith, W.H.F., Sandwell, D.T., 1995. Seafloor topography predicted from satellite altimetry and ship depth measurements. World Data Center-A for Marine Geology and Geophysics. Report MGG-09, National Geophysical Data Center, Boulder.

Snedecor, G.W., Cochran, G.C., 1980. Statistical Methods. 7th edn. Iowa State Univ. Press, 507 pp.

Stein, S., Woods, D.F., 1989. Seismicity: mid-ocean ridge. In: James, D.E. (Ed.), Encyclopedia of Solid Earth Geophysics. Van Nostrand-Reinhold, New York, pp. 1050–1054.

Stewart, L.M., Okal, E.A., 1983. Seismicity and aseismic slip along the Eltanin Fracture Zone. J. Geophys. Res. 88, 10495–10507.

Stock, J.M., Molnar, P., 1982. Uncertainties in the relative positions of the Australia, Antarctica, Lord Howe, and Pacific plates since the Late Cretaceous. J. Geophys. Res. 87, 4697–4714.

Talandier, J., Okal, E.A., 1984a. The volcanoseismic swarms of 1981–1983 in the Tahiti–Mehetia area, French Polynesia. J. Geophys. Res. 89, 11216–11234.

Talandier, J., Okal, E.A., 1984b. New surveys of Macdonald Seamount, Southcentral Pacific, following volcanoseismic activity, 1977–1983. Geophys. Res. Lett. 11, 813–816.

Talandier, J., Okal, E.A., 1996. Monochromatic T waves from underwater volcanoes in the Pacific Ocean: ringing witnesses to geyser processes?. Bull. Seismol. Soc. Am. 86, 1529–1544.

Talandier, J., Okal, E.A., Craig, H., 1988. Seismic and in situ observations of Macdonald Seamount Eruption, 11 October 1987. EOS, Trans. Am. Geophys. Union 69, 258–259, (Abstract).

Vlastelic, I., Dosso, L., Guillou, H., Bougault, H., Géli, L., Etoubleau, J., Joron, J.-L., 1998. Geochemistry of the Hollister Ridge: relation with the Louisville hotspot and the Pacific–Antarctic Ridge. Earth Planet. Sci. Lett. 160, 777–793.

Wessel, P., Kroenke, L.M., 1997. A geometric technique for relocating hotspots and refining absolute plate motions. Nature 387, 365–369.

Wessel, P., Smith, W.H.F., 1991. Free software helps map and display data. EOS, Trans. Am. Union 72, pp. 441 and 445–446.

Wolfe, C.J., Bergamn, E.A., Solomon, S.C., 1993. Oceanic transform fault earthquakes with unusual mechanisms or locations: relation to fault geometry and state of stress in adjacent lithosphere. J. Geophys. Res. 98, 16187–16211.

Wysession, M.E., Okal, E.A., Miller, K.L., 1991. Intraplate seismicity of the Pacific Basin, 1913–1988. Pure Appl. Geophys. 135, 261–359.